Author Manuscript

Published in final edited form as:

Journal of Biomaterials Applications 35 (4-5) 471-484

Doi: 10.1177/0885328220940194

Title:

Electrospinning of bioactive polycaprolactone-gelatin nanofibres with increased pore size for cartilage tissue engineering applications

Ângela Semitela[a], André F. Girão[a], Carla Fernandes[a], Gonçalo Ramalho[a], Igor Bdikin[a], António Completo[a]* and Paula A.A.P. Marques[a]*

[a] TEMA, Department of Mechanical Engineering, University of Aveiro, Campus Universitário de Santiago, 3810-193 Aveiro, Portugal

*** Corresponding Author:**

Paula A.A.P. Marques and António Completo
E-mail addresses: paulam@ua.pt and completo@ua.pt

Abstract

Polycaprolactone (PCL) electrospun scaffolds have been widely investigated for cartilage repair application. However, their hydrophobicity and small pore size has been known to prevent cell attachment, proliferation and migration. Here, PCL was blended with gelatin (GEL) combining the favorable biological properties of GEL with the good mechanical performance of the former. Also, polyethylene glycol (PEG) particles were introduced during the electrospinning of the polymers blend by simultaneous electrospraying. These particles were subsequently removed resulting in fibrous scaffolds with enlarged pore size. PCL, GEL and PEG scaffolds formulations were developed and extensively structural and biologically characterized. GEL incorporation on the PCL scaffolds led to a considerably improved cell attachment and proliferation. A substantial pore size and interconnectivity increase was obtained, allowing cell infiltration through the porogenic scaffolds. All together these results suggest that this combined approach may provide a potentially clinically viable strategy for cartilage regeneration.

Keywords: Cartilage tissue engineering; Electrospun scaffold; Polycaprolactone; Gelatin; Pore size; Electrospraying-generated microparticles

1. Introduction

Due to the limited regeneration ability of the cartilage tissue, several tissue engineering (TE) strategies have been used to try to develop functional tissue replacements, using scaffolds, cells and mechanical stimulus [1]. Still, the success of the those strategies rely on the development of appropriate scaffolding structures similar to the anisotropic organization of the cartilaginous tissue and the identification of appropriate cell sources, which are yet to be determined [2]. To ensure the suitability for TE applications of any scaffold, critical requirements must be met, such as biocompatibility; biodegradability to allow its replacement with native tissue; porosity to enable oxygen, nutrients and waste diffusion and exchange; and mechanical properties consistent with the anatomical site in which they will be implanted [3,4]. Electrospinning has been widely used to produce fibrous scaffolds for cartilage repair, not only due to the resemblance with the native nanoscale extracellular matrix (ECM) present on the cartilaginous tissue, but also because it is quite easy to manipulate the scaffold properties [5–11]. Beside the inherent fibrous features displayed by these scaffolds, the characteristics of the polymers used will determine several properties, such as hydrophobicity, hydrophilicity, mechanical strength and cell-scaffold interactions [12]. Among the synthetic polymers, polycaprolactone (PCL) is a FDA approved biocompatible and biodegradable polymer with excellent mechanical properties, easy to process and tailor to provide a wide range of physical properties [13,14]. However, due to its inherent hydrophobicity and absence of natural bio-inductive abilities, PCL-based scaffolds can lower or prevent cell attachment and proliferation [15]. Composite fibrous scaffolds made of synthetic and natural polymer blends combine the favorable and desired biological features of natural polymers with the mechanical performance of the synthetic ones [16]. Gelatin (GEL) is a natural polymer derived from collagen, the major component of the native ECM, which has been widely used for TE purposes due to its relatively easy availability, low cost and biodegradability [16]. Since the first report of electrospun PCL+GEL scaffolds by Zhang *et al* [17], this composite has been widely used as a versatile biomimetic substrate to the regeneration of a variety of tissues [18–21]. However only a few studies have reported the use of this composite for cartilage TE [6,22,23].

Despite the potential of the fibrous scaffolds for cartilage tissue repair, a significant limitation is the inherent small pore size by which these structures are characterized [24]. While their high porosity and large surface area to volume ratio are known to be beneficial to cell attachment and proliferation, their pore size, much smaller than the actual chondrocyte size (10 to 20 μm [25]) may prevent cell migration and scaffold colonization, relegating tissue formation to the surface [24,26]. To overcome this limitation, several investigators have proposed mechanisms for increasing the average pore size of electrospun scaffolds. The combination of micro and nanofibers in scaffolds generated a wide range of pore distributions which allowed infiltration of different types of cells, but the reduction of the number of nanofibers affected cell spreading [27]. Cryogenic electrospinning has also been used with satisfactory results, however this approach require a very complex electrospinning set-up [28]. Salts and other soluble particles with varying diameters have been integrated as sacrificial components in fibrous scaffolds to increase pore size [7]. NaCl particles integrated and later removed from electrospun scaffolds has produced promising cell infiltration results, however this technique also requires an unusual electrospinning set-up to allow particle deposition on top of the electrospun scaffold [29]. Another mechanism to increase the average pore size of nanofibrous scaffolds is the co-electrospinning or electrospraying of sacrificial materials, such as polyethylene oxide (PEO) or polyethylene glycol (PEG), with the polymer of interest [24]. The sacrificial polymer is then removed by immersion in a solvent that has no effect on the structure of the polymer of interest, leaving large pores and interfibre spacing in the final scaffold. The porosity can be tuned by carefully selecting the sacrificial polymer, its molecular weight and its flow rate, which can alter the fiber or particle diameter and deposition [24]. Using this approach, Baker *et al* increased scaffold porosity by co-electrospinning PCL, a

slowly degrading material, and PEO, an aqueous soluble material, as cell infiltration improved with rinsing PEO content [30]. Wang *et al* combined PCL electrospinning with PEO electrospraying, obtaining a 2 and 3-fold rise of the pore size of electrospun PCL scaffolds [31]. Most work to date using sacrificial components on electrospun scaffolds is limited to synthetic polymers [24]. If a blend of synthetic and natural polymer, such as PCL+GEL, would be used, we hypothesized that the porosity of the final PCL+GEL scaffolds might be intensified by a gradual dissolution of GEL component, which will further improve cell infiltration.

This study introduces a new engineering approach by combining the incorporation of GEL on electrospun PCL scaffolds and the introduction of a sacrificial material – PEG – to create porogenic scaffolds. This combination will allow not only improved cell attachment and proliferation, but also of cell migration. So, a series of electrospun scaffolds composed of PCL, GEL and PEG sacrificial particles were fabricated and characterized on their fibrous morphology, physicochemical properties, mechanical behavior and biocompatibility.

2. Materials and methods

2.1. Preparation of scaffolds with different formulations

PCL (80kDa, Sigma-Aldrich) and GEL from porcine skin (Sigma-Aldrich) were dissolved separately in 2,2,2-trifluoroethanol (TFE, TCI) at a concentration of 10% (wt/v) and stirred vigorously at room temperature overnight. Before electrospinning, the two solutions were mixed in 50:50 volume ratio (PCL+GEL) and 0.2% (v/v) of acetic acid (Sigma-Aldrich) was added to facilitate the mixture. A 10% (wt/v) PCL solution was also prepared in a solution of TFE: Dimethylformamide (DMF, Fisher Scientific) (75:25 v/v) for comparison (Fig. S1) and stirred vigorously at room temperature overnight. The solutions were placed in 5 mL plastic syringe within the electrospinning machine (NANON 01, MECC), and fed at a controlled flow rate of 1.5 mL/h to a blunt needle with a tip diameter of 0.8 mm (21G), with applied voltage of ~ 27 kV. The polymer jet was ejected onto a rotating drum (20 cm width and 20 cm diameter) at 750 rpm using a needle to collector distance of 9 cm (Figure 1a). The prepared scaffolds were dried for 1 week at room temperature to remove residual solvent before subsequent use. To prepare the porogenic scaffolds, a PEG solution (1.5 g/mL) was prepared by dissolving the PEG (8kDa, Sigma-Aldrich) in chloroform (ACROS Organics) and stirring at 50 ºC for 30 min. The solution was allowed to cool down at room temperature for 10 minutes, and then poured into a 5 mL plastic syringe and electrosprayed simultaneously with the 10% (wt/v) PCL and 10% (wt/v) PCL+GEL solutions, using the same parameters of the previous set up as exemplified in Figure 1b. To intensify the impact of the sacrificial agent the selected flow rate was 4 mL/h and a needle with a tip diameter of 1.2 mm (18G) was used. The PEG particles were removed from the PCL+PEG and PCL+GEL+PEG scaffolds by immersion in a graded series of ethanol aqueous solutions (90, 70, 50, 30 and 10% v/v) and then in distilled water. Afterwards, the scaffolds were freeze-dried (LyoQuest, Telstar). These scaffolds will from now on be referred as PCL+PEG and PCL+GEL+PEG when PEG particles are still present, and PCL porogenic and PCL+GEL porogenic after PEG removal. The thicknesses of the scaffolds, measured with the aid of a micrometer, were approximately the following: 115 μm for PCL, 110 μm for PCL+GEL, 130 μm for PCL porogenic and 180 μm for PCL+GEL porogenic.

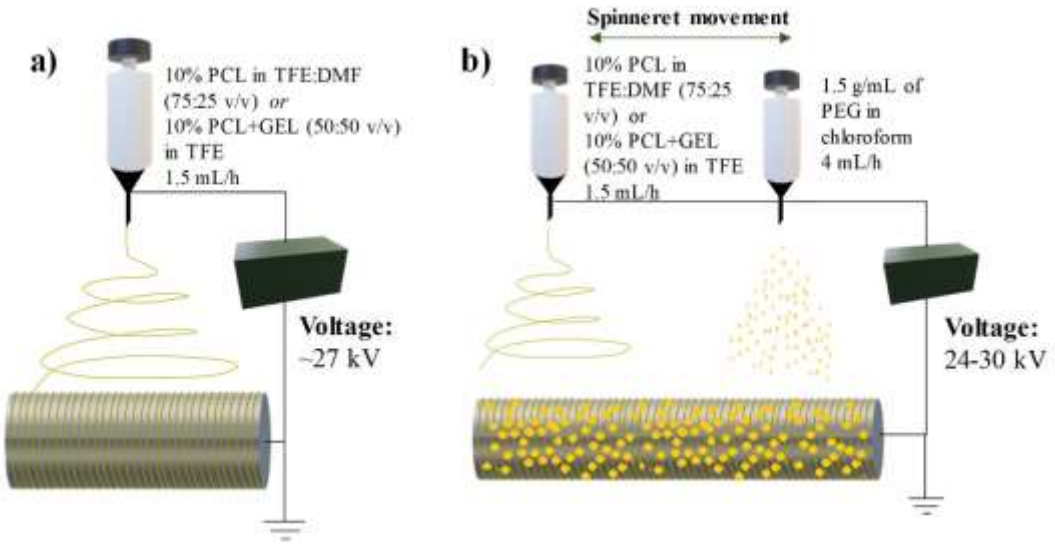

Figure 1. Illustrative diagram of the electrospinning set-ups used to:(a) electrospun 10% (wt/v) PCL and 10% (wt/v) PCL+GEL scaffold formulations and (b) incorporate PEG particles by co-electrospinning with 10% (wt/v) PCL and 10% (wt/v) PCL+GEL formulations.

2.2. Characterization of scaffolds

2.2.1. Scanning electron microscopy (SEM)

The morphology of fibrous scaffolds, without PEG and with PEG (before and after PEG removal), was visualized via SEM (Hitachi TM4000 plus, Japan) at an accelerating voltage of 5 kV. Based on the SEM images, fiber diameter and pore size distributions were determined using Image J-Pro Plus software: fibers diameter was analyzed manually by measuring the diameters of over 100 randomly selected fibers of each scaffold formulation (n > 100); pores sizes were manually measuring over 50 randomly selected areas between the fibers (n > 50).

2.2.2. Porosity measurements

The porosity of the PCL, PCL+GEL and the respective porogenic scaffold formulations was estimated using a published method [32,33]. Briefly, scaffolds (n = 3) were weighted and size measured to calculate the apparent density by the equation (1).

$$apparent\ density\ (g/cm^3) = \frac{scaffold\ mass\ (g)}{scaffold\ thickness\ (cm) \times scaffold\ area\ (cm^2)} \quad (1)$$

Porosity was then calculated through the ratio of the apparent and bulk densities of the materials of the scaffolds (bulk densities of 1.145 g/cm^3 and 1.3 g/cm^3 for PCL and GEL, respectively) (2).

$$Scaffold\ porosity\ (\%) = 1 - \frac{scaffold\ apparent\ density (g/cm^3)}{scaffold\ bulk\ density\ (g/cm^3)} \times 100 \quad (2)$$

2.2.3. Attenuated total reflectance fourier transform infrared spectroscopy (ATR-FTIR)

The chemical structure of scaffolds was determined by ATR-FTIR (Perkin Elmer Spectrum BX, USA) from 4000-500 cm^{-1} with a resolution of 8 cm^{-1} and 32 scans. GEL and PEG powders' chemical structure were also analyzed to confirm GEL presence and PEG incorporation and subsequent removal, respectively.

2.2.4. Water contact angle

Assessment of the wettability of the PCL, PCL+GEL and the respective porogenic formulations was performed measuring water contact angle (n = 3) by static contact angle using the sessile

drop method (drop volume of 3 μL) and the shape of the liquid–vapor interface was determined by the Young–Laplace equation. The measurements were carried out with OCA 20 (DataPhysics Instruments, Germany) at room temperature.

2.2.5. Hydraulic permeability

The hydraulic permeability of the PCL, PCL+GEL and the respective porogenic formulations was determined using Darcy's law [34]. The scaffolds were placed in a permeability measuring setup and a continuous water pressure was applied on the scaffolds for 10 minutes. The flushed water was then collected from the outlet and weighed. For the control, no scaffold was placed between the flow-path. The hydraulic permeability, k ($m^4\ N^{-1}\ s^{-1}$) was calculated by applying the obtained values to the equation (3).

$$k = \frac{Scaffold\ thickness\ (m)}{Flushing\ area\ (m^2) \times Outlet\ water\ mass\ (g)} \times \frac{2\pi^2 Flushing\ area\ radius\ (m)^4}{(Control\ water\ mass\ (g)/Outlet\ water\ mass\ (g))^2 - 1} \quad (3)$$

2.2.6. Mechanical testing

Tension. Rectangular-shaped samples of the scaffolds were stretched, using a Shimadzu MMT-101N (Shimadzu Scientific Instruments, Japan) with a load cell of 100 N, at a constant cross-head speed of 10 mm/min under dry and wet conditions (n = 6). The Young's moduli of the samples were calculated through the tangent modulus of the linear portion of the stress–strain curve obtained. Linearity for Young's moduli possessed a $R^2 > 0.95$.

Nanoindentation. Nanoindentation was performed (TTX-NHT, CSM instruments Nanoindenter) at room temperature, with a three-side pyramidal Berkovich diamond indenter having nominal edge radius 20 nm (faces 65.3° from vertical axis). Nanoindentation measurements (n = 3) were conducted as follows: a load rate of 1000 mN/min was applied, until a maximum load of 50 mN was reached and held during 10 s; then the indenter was withdrawn at an unloading rate of 1000 mN/min. Elastic modulus and hardness of scaffolds were calculated based on the Oliver and Pharr method [35].

2.2.7. *In vitro* degradation assessment

The *in vitro* degradation analysis of the PCL and PCL+GEL scaffolds was carried out by incubating the scaffolds, with known weights, in Phosphate-Buffered Saline (PBS, 1x; Sigma-Aldrich) at 37 ºC for 14 days. Before the procedure, the PCL and PCL+GEL scaffolds were gradually hydrated at room temperature through a graded series of ethanol aqueous solutions (90, 70, 50, 30 and 10% v/v)– to simulate the washes that the scaffolds are subjected upon PEG removal, and then placed in PBS at 37 ºC. PCL+GEL scaffolds were also place immediately in PBS to access the influence of the ethanol treatment on GEL depletion (PCL+GEL I). After the hydration step (3 hours) and 1, 3, 7 and 14 days of incubation, samples (n = 3) of each condition were removed, washed in distilled water and freeze-dried. Afterwards samples were weighted, and the percentage of polymer content left in the scaffold was calculated (4). Samples were also visualized in SEM, as previously described.

$$Polymer\ content\ (\%) = \left(1 - \frac{Initial\ weight\ (g) - Final\ weight\ (g)}{Initial\ weight\ (g)}\right) \times 100 \quad (4)$$

2.2.7.1. Picrosirius red staining

GEL retention was detected by a picrosirius red staining. Briefly, scaffolds were washed in PBS and stained with 0.5 mg/mL picrosirius red (Direct red 80 dye; Sigma-Aldrich) in saturated picric acid (Sigma-Aldrich) for 1 hour, washed with 0.5 % acidified water, dehydrated in 95 and 100 % (v/v) ethanol aqueous solutions, cleared in xylene and visualized and visualized in an optic microscope (Nikon Eclipse LV150).

2.3. Biocompatibility evaluation of the scaffolds

2.3.1. Cell culture and seeding

An articular cartilage progenitor cell line (CP5, Sigma–Aldrich) was used to access the scaffolds' biocompatibility. Cells were maintained at 37 ºC in a humidified atmosphere of 5% CO_2 in air, in Dulbecco's Modified Eagle's Medium/Nutrient Mixture F-12 Ham (DMEM/F-12, Sigma–Aldrich), supplemented with 10% (v/v) fetal bovine serum (FBS, Sigma–Aldrich) and 1% (v/v) penicillin/streptomycin (P/S, Sigma–Aldrich). The medium was refreshed three times a week. Cells were harvested at pre-confluence using Trypsin/EDTA solution (0.25%, Sigma-Aldrich). Scaffolds were sterilized in 70% ethanol aqueous solution (v/v) for 4 hours and then washed in PBS 3 times. Scaffolds were then placed in a 24-well plate. Cells were seeded at $0.25x10^6$ cells per scaffold followed by incubation at 37 ºC for 2 h to allow cell attachment. Afterwards, fresh medium was added until it reached a final volume of 1 mL per well.

2.3.2. Cell metabolic activity

A resazurin method was used to assess cell metabolic activity after 1, 3, 7 and 14 days. Resazurin solution (0.1 mg/mL in PBS, ACROS Organics) was added to fresh medium at a final concentration of 10% (v/v). Scaffolds were incubated in this solution at 37 ºC for 4 h in the dark, after which 100 µL per well was transferred to a 96-well plate and absorbance (Abs) at 570 and 600 nm was measured (n = 3 for each group) in a microplate reader (Synergy HTX, BioTek). For each day, final absorbance values for each sample were calculated as the ratio Abs570/Abs600 nm minus the Abs570/Abs600 nm ratio of a negative control (scaffold without cells). The absorbance values of cells incubated in the tissue culture polystyrene on the first time point were taken as 100% and the percentage of viable cells was calculated from these control values.

2.3.3. Cell morphology and infiltration

Cell-laden scaffold formulations were fixed with 4% (wt/v) formaldehyde (ACROS Organics) in PBS and cell morphology and infiltration into the scaffolds were accessed. SEM was used to visualize cell morphology. Briefly, samples were dehydrated via graded concentrations of ethanol aqueous solutions (50, 70, 90, 95 and 100% v/v), dried with hexamethyldisilane (TCI, Japan), mounted and observed using a Hitachi TM4000 plus at an accelerating voltage of 5 kV. Cell infiltration was accessed through a DAPI (4',6-diamidino-2-phenylindole, Sigma) staining of the nucleus, and visualized using a fluorescence microscope (Axioimager M2, Zeiss) with magnification of 20x/0.50. Afterwards, cell infiltration was quantified using Image J-Pro Plus software: distance between randomly selected cell nucleus (n = 20 per scaffold formulation) and the scaffolds' surface were manually measured.

2.4. Statistical analysis

All the quantitative data are expressed as mean ± standard deviation. Statistical significance was determined, using OriginLab, by performing One-way analysis of variance (ANOVA), followed by post hoc Tukey's test, except for viability assays, where a One-way ANOVA with repeated measures was also used. Significance was accepted at p-values inferior to 0.001, 0.01 and 0.05.

3. Results and discussion

3.1. Morphology of the electrospun fibrous scaffolds

All formulations were successfully electrospun (Figure 2). It should be noted that in order to obtain uniform and beadless PCL fibers using TFE, it was necessary to add DMF to the solvent system, (Figure S1). PCL+GEL fibers were smoother, more uniform and possessed significantly lower fiber diameters (0.30 ± 0.07 μm) than the PCL fibers (0.69 ± 0.19 μm) (Figure 2a, b, and c). In reality, since GEL has higher density (1.3 g/cm^3) than PCL (1.13 g/cm^3), GEL incorporation on the PCL solution allowed the preservation of an optimum viscous behavior, and consequently, prevented capillary instabilities of the jet at the tip of the needle [19,36]. Furthermore, the average fiber diameter of PCL+GEL scaffolds falls within the range of values reported for type II collagen fibrils (100 nm to 300 nm) [36–38]. Still, despite the potential stimulatory effect of such small fibers, they greatly reduced the scaffolds' pore sizes, particularly for PCL+GEL (3.97 ± 1.15 μm; Figure 2j) where 65 % of the pores were smaller than 5 μm. PCL scaffolds, on the other hand, possessed bigger pores (6.23 ± 1.85 μm; Figure 2i) that ranged mostly from 5 to 10 μm (80%). Nonetheless, since adequate pore sizes determine the degree of cell migration into the scaffold, and ultimately the scaffolds' *in vitro* and *in vivo* performance, and chondrocyte diameters range from 10 to 20 μm [25,39], it was required an optimization of this parameter. In this regard, PEG sacrificial particles were simultaneously electrosprayed with each spinning solution (Figure 2d and e). Spherical particles with a broad diameter distribution were obtained (Figure 2f), with average sizes of 17.66 ± 9.98 μm for PCL+PEG and 17.98 ± 11.26 μm for PCL+GEL+PEG. These PEG particles were then removed, creating porogenic scaffolds with large interfibre spaces (Figure 2g and h). Pore sizes were substantially higher on scaffolds after PEG particles removal, with a 2 and 3-fold increase of the average pore size value from PCL to PCL porogenic (12.46 ± 5.62 μm; Figure 2i) and from PCL+GEL to PCL+GEL porogenic scaffolds (14.27 ± 4.23 μm; Figure 2j), respectively. A slight difference was also observed between both porogenic formulations pore sizes, which could be attributed to an additional GEL dissolution from PCL+GEL porogenic scaffolds [17]. It should be noted that in order to preserve the 3D structure of the porogenic scaffolds, a gradual ethanol-based hydration was performed, as ethanol is a non-solvent for PEG at room temperature [37]. This procedure was particularly crucial to the hydrophilic GEL-containing scaffolds, since GEL is insoluble in ethanol [40]. Indeed, upon first contact with high concentration ethanol solutions, GEL stablishes bonds with ethanol molecules, creating ethanol sandwich clusters with the layer of water molecules inside, which ultimately leads to fiber dispersion, and preservation of the fibrous structure [41]. This way GEL fiber fusion as well as rapid and excessive GEL dissolution can be prevented [31], which in fact was confirmed by the biodegradation studies on the PCL+GEL (Figure S2). The dissolved amount of GEL was lower (~ 40 %) on the PCL+GEL scaffolds subjected to the ethanol hydration treatment compared to the PCL+GEL controls, immersed only in PBS (~ 50%) (Figure S2a). In fact, these results suggest that virtually no GEL remained in the scaffolds when the referred treatment was not employed, which is consistent not subjected to the referred treatment, which was consistent with the polymer mass loss results. Furthermore, the SEM images of the degraded samples confirmed the reduced GEL fiber fusion on the PCL+GEL scaffolds subjected to the ethanol hydration treatment, and increased fiber dispersion attributed to the referred ethanol sandwich clusters (Figure S2b).

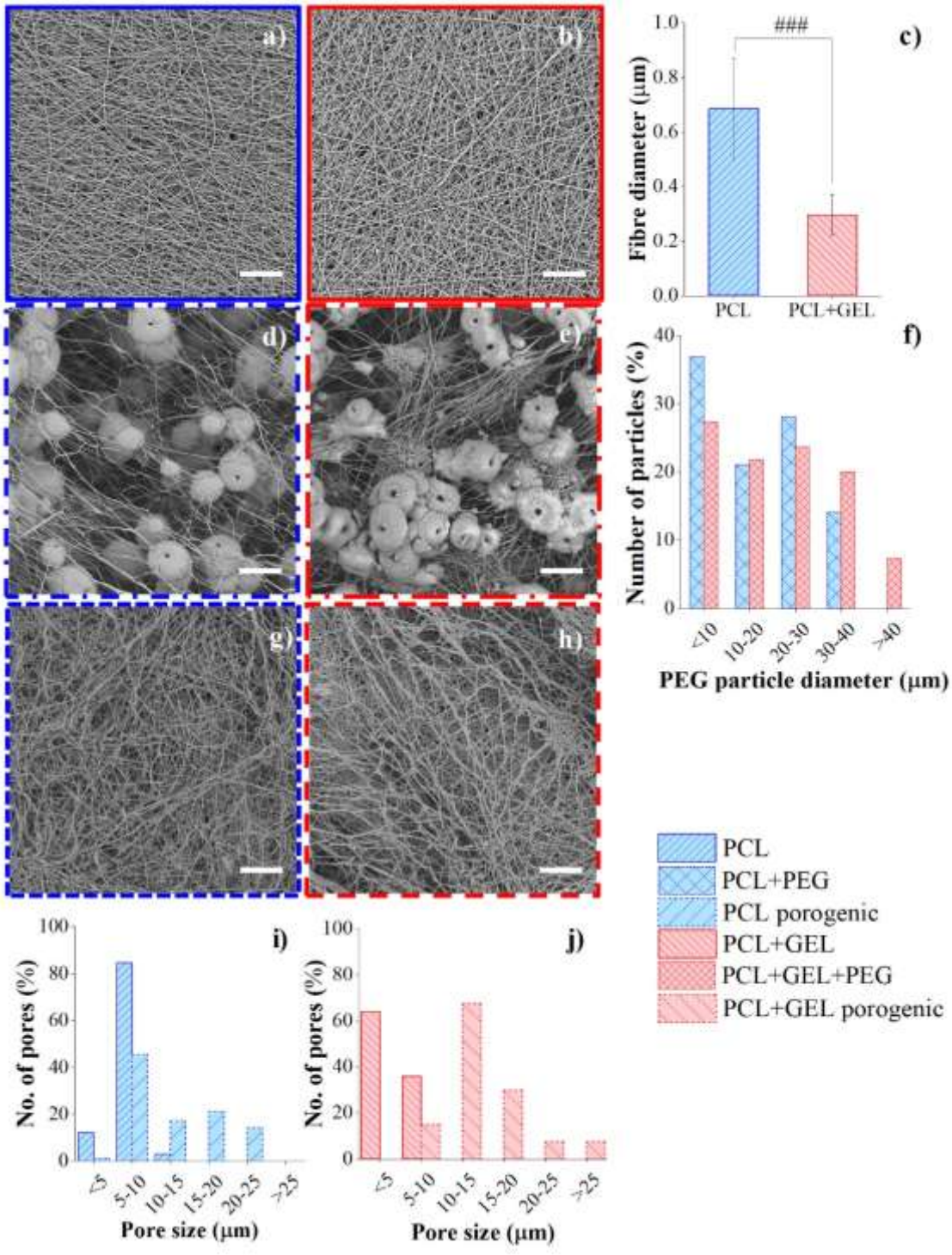

Figure 2. SEM images of PCL (a), PCL+PEG (d), PCL porogenic (g), PCL+GEL (b), PCL+GEL+PEG (e) and PCL+GEL porogenic (h) fibrous scaffolds; fibre diameter of PCL and PCL+GEL scaffolds (c); PEG particle diameter distribution of PCL+PEG and PCL+GEL+PEG scaffolds (f); pore size distributions of PCL and PCL porogenic (i), and PCL+GEL and PCL+GEL porogenic scaffolds (j). Scale bar: 30 µm. Statistical analysis by One-way ANOVA followed by post hoc Tukey's test; ###p <0.001.

3.2. Physicochemical characterization of the fibrous scaffolds

Table 1 summarizes the main physical properties of the developed scaffolds: thickness, porosity, hydraulic permeability and water contact angles. The porogenic scaffolds were thicker than the regular ones, implying that the PEG removal procedure preserved the 3D porogenic arrangement. Furthermore, higher porosities were registered on the porogenic scaffolds in relation to their respective regular scaffolds. In fact, PCL+GEL porogenic displayed the highest porosity, which can be attributed not only to the improved pore sizes, but also to the GEL dissolution after PEG removal. A similar trend was observed for the scaffolds' hydraulic permeability. Even though the registered permeability values were considerably higher than those reported for articular cartilage (10^{-16} to 10^{-15} $m^4/N{\cdot}s$ [43]), they imply the presence of an enhanced pore interconnectivity that allowed water flow that is, ultimately, expected to facilitate nutrient supply and waste removal *in vitro* [44,45]. The water contact angle measurements revealed that scaffolds became hydrophilic with the incorporation of GEL (from 130.20 ± 4.18 ° of the PCL to 29.53 ± 1.80 ° of PCL+GEL scaffolds), due to presence of the amine and carboxyl function groups in the GEL structure [21]. Since cell adhesion occurs preferably in hydrophilic surfaces, it is expected an improved cell response to these hydrophilic scaffolds [5,19–21]. Interestingly, the water contact angles of the PCL+GEL porogenic (43.50 ± 6.17 °) were significantly higher than the contact angle measured for the PCL+GEL scaffolds. Both increased surface roughness and GEL dissolution could have contributed to this difference. Indeed there are reports of higher contact angle in surfaces with higher porosity and roughness due to the trapped air in the interfibre space which allows the water droplets to be sustained on the surface [46]. Still, despite of the increased surface roughness of the PCL porogenic, no substantial differences of the water contact angles were found with the PCL-only based scaffold.

The infrared spectra of electrospun scaffolds are shown in Figure 3. The PCL spectra displays strong bands attributed to CH_2 stretching at 2940 cm^{-1}, 2866 cm^{-1} and 734 cm^{-1}, C=O stretching at 1720 cm^{-1}, COC stretching at 1241 cm^{-1} and 1162 cm^{-1} and O–C stretching at 1046 cm^{-1} and 961 cm^{-1} [47] (Figure 3a). The incorporation of GEL in the PCL scaffold led to the appearance of protein-related bands at 3294 cm^{-1} attributed to N–H stretching of amine bonds, and at 1647 cm^{-1} and 1543 cm^{-1} assigned to C=O stretching and the combination of N–H bending and C–N stretching of the amide bonds, respectively [12,48,49] (Figure 3a). A shifting from the original absorption bands was observed in the PCL+GEL scaffolds, suggesting a possible hydrogen bond between ester group of PCL and amine group of GEL. Indeed, the characteristic band of PCL, regarding C=O stretching and COC stretching, originally situated at 1720 and 1162 cm^{-1} were found at 1725 and 1186 cm^{-1} on PCL+GEL scaffolds, respectively. Likewise, the characteristic amide bands of GEL, regarding stretching and the C=O stretching and the combination of N–H bending and C–N stretching, originally situated at 1624 and 1532 cm^{-1} shifted to around 1647 and 1543 cm^{-1}. Similar conclusions were previously reported [50]. When PEG microparticles were added to the regular formulations, several new PEG-related bands appeared in their spectra associated with the CH_2 stretching at 2876 cm^{-1}, the CH_2 bending at 1468 cm^{-1} and 1342 cm^{-1}, the O–H and C–O–H stretching at 1278 cm^{-1} and 1096 cm^{-1} and the C–C stretching at 956 cm^{-1} and 842 cm^{-1} [51–53] (Figure 3b and c). The absence of these bands on the spectra of the porogenic scaffolds confirmed that the PEG microparticles were indeed removed (Figure 3b and c). It should also be noted that, as previously suggested, GEL continued to be present in the GEL-containing scaffolds after the PEG removal treatment (Figure 3c).

Table 1. Physical properties of the scaffolds. Statistical analysis by One-way ANOVA followed by post hoc Tukey's test; $^{###}p < 0.001$, $^{##}p < 0.01$; where ## and ### denote statistically significant difference of the referred scaffold formulation with the remaining.

Properties	PCL	PCL porogenic	PCL+GEL	PCL+GEL porogenic
Scaffold thickness (μm)	117.19 ± 11.97	130 ± 15.38	111.56 ± 23.07	181.25 ± 39.85
Porosity (%)	71.26 ± 1.96$^{##}$	75.25 ± 1.39	77.77 ± 2.14	83.48 ± 1.94$^{###}$
Hydraulic permeability ($\times 10^{-5}$ $m^4/N{\cdot}s$)	0.84 ± 0.15	1.89 ± 0.45$^{##}$	0.62 ± 0.47	3.06 ± 0.77$^{##}$
Water contact angles (°)	130.20 ± 4.18	123.87 ± 3.70	29.53 ± 1.80$^{###}$	43.50 ± 6.17$^{###}$

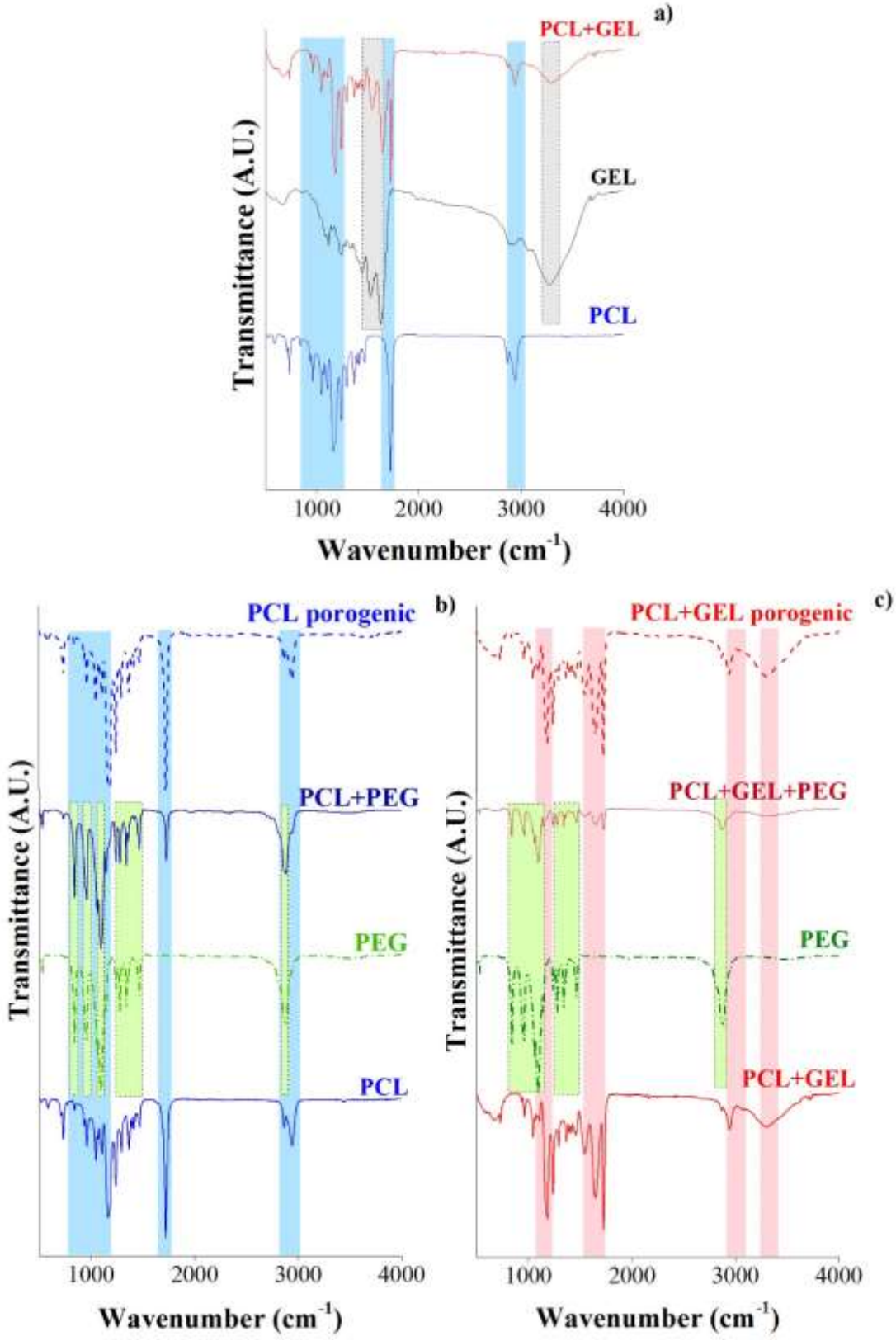

Figure 3. ATR-FTIR spectra of the PCL and PCL+GEL (a), PCL+PEG and PCL porogenic (b) and PCL+GEL+PEG and PCL+GEL porogenic (c).

3.3. Mechanical characterization of the fibrous scaffolds

The tensile mechanical properties are displayed in Figure 4a-c. The stress-strain behavior of the fibrous scaffolds in dry and wet states contained two stages – the first one corresponds to the linear elastic response followed by a non-linear plastic behavior, which generally ends with the fracture of the fibrous layer [50,54] (Figure 4a and b). Under dry conditions (Figure 4a and c), PCL+GEL scaffolds displayed higher Young's modulus (26.79 ± 6.60 MPa) than PCL alone (12.21 ± 1.15 MPa). Since GEL is a stiffer polymer, an increase of the composite Young's modulus was expected [17,38]. Also, PCL+GEL fiber diameter was considerably smaller, resulting in increased crystallinity and, consequently, higher elastic modulus [55–57]. The respective porogenic scaffolds exhibited lower Young's modulus (9.00 ± 1.60 MPa and 12.97 ± 6.54 MPa for PCL porogenic and PCL+GEL scaffolds, respectively), due to the increase of porosity [30,38]. Regarding tensile strength and elongation at break, it was not possible to compare the four scaffold formulations because most of the scaffolds tested were distensible beyond the range of the testing device. The mechanical properties of the scaffolds were also accessed under wet conditions, since these conditions reflect more closely the native physiological environment. Here, there was a substantial reduction of the tensile properties of the GEL-containing scaffolds from 26.79 ± 6.60 MPa and 12.97 ± 6.54 MPa for dry PCL+GEL and PCL+GEL porogenic to 3.20 ± 0.91 MPa and 2.23 ± 0.91 MPa for wet PCL+GEL and PCL+GEL porogenic scaffolds, respectively (Figure 4b and c). This behavior can be attributed to GEL hydrophilic character, and it was already reported for wet GEL-based nanofibrous scaffolds [6,54]. There were no significant differences between the Young's modulus of PCL scaffolds under dry and wet conditions, and for PCL porogenic scaffolds the difference was significant, which can be attributed to the increased pore size [30], but minor compared with GEL-containing scaffolds. Even though these values were substantially lower, they still fell within the range of values reported for cartilage tissue elastic modulus (2-12 MPa) [43,58].

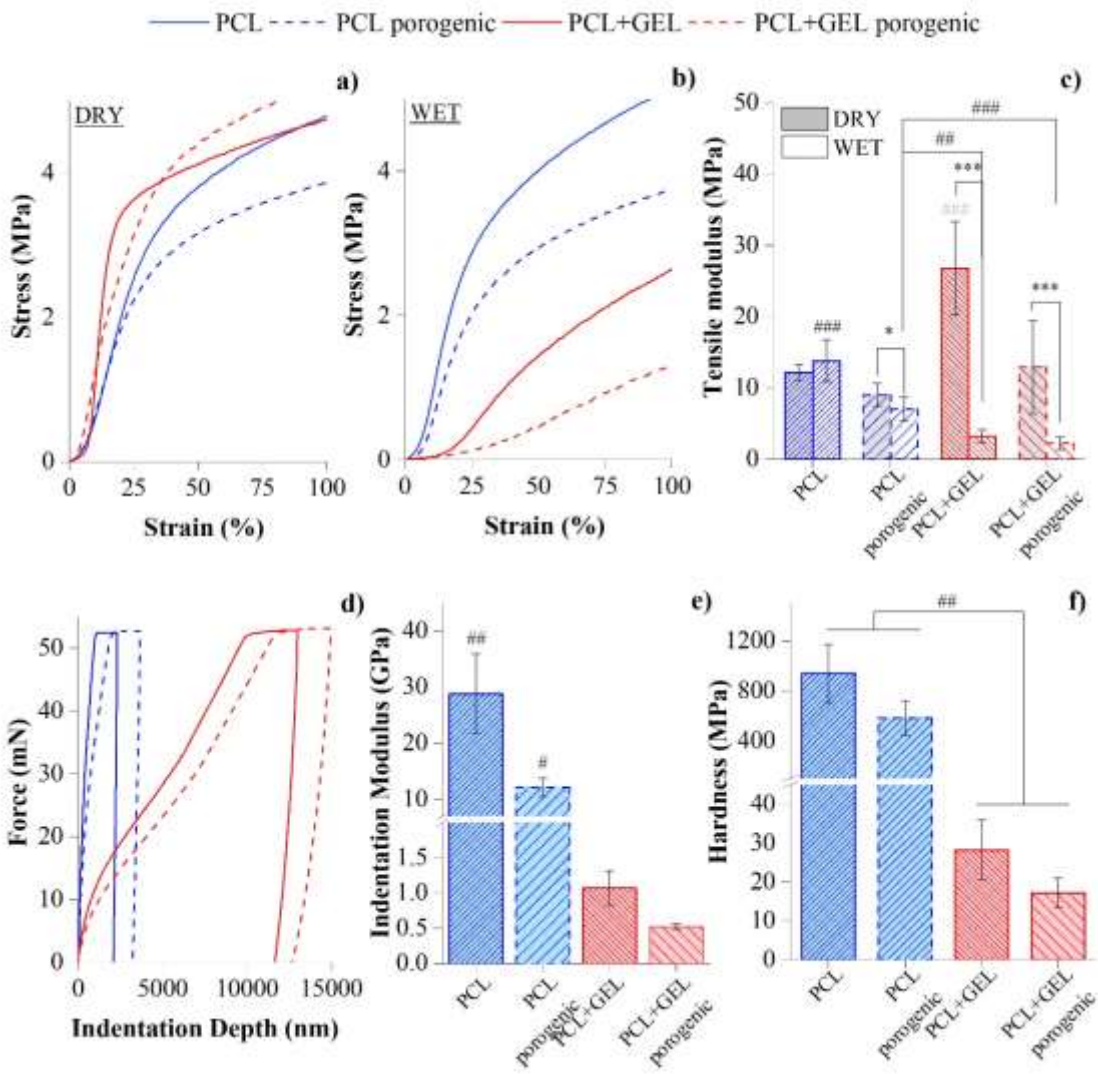

*Figure 4. Mechanical properties of the PCL, PCL porogenic, PCL+GEL and PCL+GEL porogenic fibrous scaffolds: Tensile stress-strain curves under dry (a) and wet (b) conditions and respective tensile modulus (c); load-indentation depth curves (d) and the respective indentation moduli (e) and hardness (f). Statistical analysis by One-way ANOVA followed by post hoc Tukey's test: ###p <0.001, ##p <0.01, where # denotes statistical significant differences between formulations under each condition; ***p <0.001, *p <0.05, where * denotes statistical significant differences between conditions for each formulation.*

The scaffolds' compressive properties were here assessed using nanoindentation (Figure 4d-e), given that the scaffolds were too thin for conventional compression to be conducted [43,59]. From the load-indentation depth curves (Figure 4d), it is possible to infer that the incorporation of GEL into the PCL scaffold formulations significantly increased the maximum penetration depth, which can be attributed to a possible fiber softening upon GEL addition. This conclusion was confirmed by the calculations of the indentation modulus and hardness (Figure 4d and e). Indeed, significantly lower moduli were registered for GEL-containing scaffolds (1.07 ± 0.24 GPa and 0.52 ± 0.03 GPa for PCL+GEL and PCL+GEL porogenic, respectively) in comparison to the PCL-based scaffolds (28.76 ± 7.14 GPa and 12.14 ± 1.65 GPa for PCL and PCL porogenic, respectively). Similar conclusions have been obtained through the compression of 3D printed PCL+GEL scaffolds, implying that the incorporation of a natural polymer can degrade the compression elastic modulus [60]. Furthermore, a statistically significant different indentation moduli was observed between regular and porogenic scaffolds, inferring a substantial impact on the compressive mechanical properties of the scaffolds upon pore enlargement. Likewise, the

hardness of the GEL-based scaffolds was significantly lower (28.20 ± 7.64 MPa and 17.18 ± 3.84 MPa for PCL+GEL and PCL+GEL porogenic as opposed to 940.97 ± 231.97 MPa and 583.67 ± 138.32 MPa for PCL and PCL porogenic, respectively). Assuming 0.001 – 6 MPa and 40 – 140 MPa to be the range of the indentation and compression modulus of native articular cartilage, respectively [9,61,62], GEL-containing scaffold formulations better approximate the required compressive properties, suggesting its potential for cartilage TE.

3.4. Biocompatibility evaluation of the fibrous scaffolds

An important aspect to prescreen the biocompatibility of a scaffold is to access its general cytotoxicity towards cells cultured *in vitro* [6]. A non-toxic resazurin metabolic assay was used to access the percentage of viable articular cartilage progenitor cells on PCL, PCL porogenic, PCL+GEL and PCL+GEL porogenic fibrous scaffolds after 1, 3, 7 and 14 days of culture, through the internalization and metabolic reduction of resazurin, a blue poorly fluorescent dye, to resorufin, a highly fluorescent compound, detected by spectrophotometry [63]. The results, shown in Figure 5a, indicate that initial cell attachment was substantial for the four scaffold formulations. PCL+GEL scaffolds displayed a significantly higher cell viability at the beginning of the culture time, suggesting that the presence of GEL was beneficial to improve cell attachment, not only due to the GEL hydrophilic character, but also to the presence of cell recognition domains (RGD) on its structure [5,6,17]. The percentage of viable cells increased significantly on the four scaffold formulations throughout the culture period, indicating that cell proliferation occurred. As previously referred, the topographic features of these constructs can have a beneficial impact of cell behavior [64]. By day 7, the percentage of viable cells on GEL-containing scaffolds was considerably higher. By day 14, a cell viability plateau was reached for PCL+GEL scaffolds, possibly implying that the cell proliferation rate decreased due to cell contact growth inhibition – scaffold saturation [63]. On the contrary, the percentage of viable cells on porogenic scaffolds continued to increase, suggesting these scaffolds, due to their enlarged pore size and improved pore interconnectivity, possessed considerably more surface area for cells to spread and migrate. SEM images of the cell-laden scaffolds (Figure 5c) revealed that cells adhered and spread well through the surface of all scaffolds, exhibiting multiple filopodia attached to the surface. It is even possible to clearly visualize the nucleus of the cells. There were no visible differences of cell morphology between PCL, PCL+GEL and PCL porogenic scaffolds. However, in PCL+GEL porogenic scaffolds, it appears that cells penetrated through the scaffold, as it is possible to distinguish fibers on top of the cells layer. Several studies have reported this migration pattern on scaffolds developed with this porogenic approach [30,65]. It is interesting to note that on PCL porogenic scaffolds, also with increased pore size, this behavior was not clearly visible, which could be associated with the absence of GEL and the respective functional peptide sequences necessary for integrin binding [66]. A small degree of GEL dissolution on PCL+GEL porogenic scaffolds may also be responsible. The enlarged pore size of PCL+GEL porogenic may also explain why this 3D migration pattern was not prominently observed on the PCL+GEL scaffolds, where cell migration was relegated to the surface. A similar trend was observed through the DAPI staining of the cell-seeded scaffolds, also displayed in Figure 5c. Unmistakably, a higher degree of cell infiltration was observed on the porogenic scaffold formulations (29 and 80 % for PCL porogenic and PCL+GEL porogenic, respectively), with a statistically significant difference from the respective regular scaffold formulations (9 and 11 % for PCL and PCL+GEL, respectively) (Figure 5b). Furthermore, once again, PCL+GEL porogenic scaffolds displayed the highest cell infiltration.

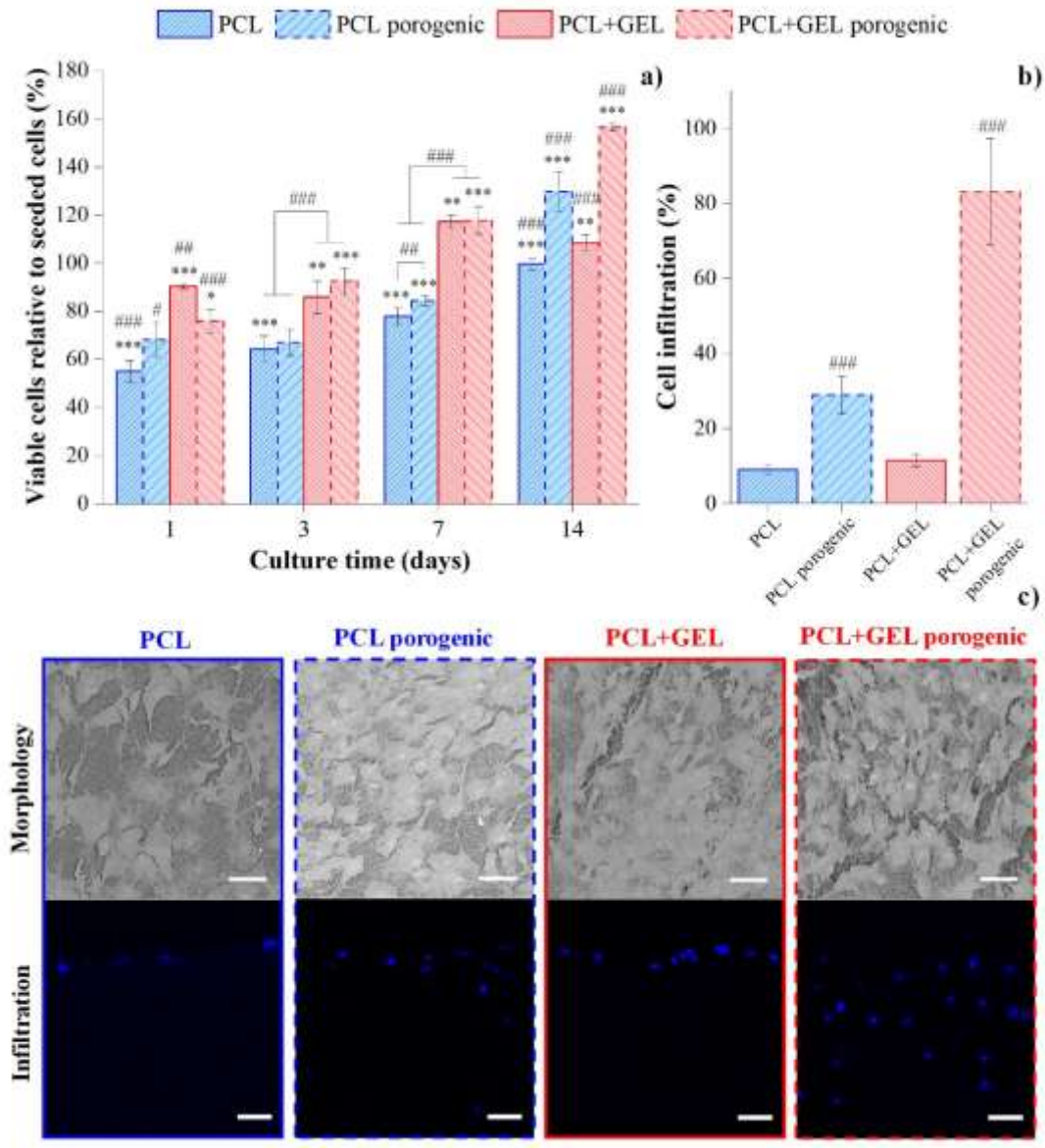

*Figure 5. In vitro studies: percentage of viable articular cartilage progenitor cells seeded on the scaffolds after 1, 3, 7 and 14 days of culture (a); and respective quantification of the cell infiltration after 14 days (b); SEM images and immunocytochemistry of nuclei (DAPI) of articular cartilage progenitor cells seeded on the scaffolds after 14 days of culture, scale bars: 50 µm. Statistical analysis by One-way ANOVA followed by post hoc Tukey's test: ***p <0.001, **p <0.01, where * denotes statistical significant differences of each formulation over time; ###p <0.001, ##p <0.01, #p <0.05, where # denotes statistical significant differences between formulations on each culture period.*

4. Conclusion

Here, an innovative engineering combined approach was developed to overcome two significant limitations of the PCL electrospun scaffolds for cartilage repair, their lack of bio-inductive properties and their characteristic small pore size. This methodology consists on incorporating a natural polymer – GEL – and a sacrificial material – PEG, later removed by immersion in water – to the PCL scaffolds. GEL was successfully blended with PCL, and the resulting composite scaffolds possessed improved wettability, resulting in better cell attachment and proliferation. The porogenic scaffolds developed had indeed increased pore size and interconnectivity, that

allowed a significantly higher degree of cell infiltration into the scaffold, and the achievement of a more homogeneous cell distribution, which ultimately might generate functional tissue replacement, *in vitro* or after *in vivo* implantation. Even though further work should be done to optimize this combined approach, these results demonstrate that this innovative methodology has great potential for scaffold development for cartilage TE applications. For future work, it is intended to use the best scaffold formulation – PCL+GEL porogenic –for the development of three-dimensional anisotropic scaffolds with a depth-dependent organization of the fibers, mimicking the articular cartilage arcade-like collagen arrangement.

Acknowledgments

The authors would also like to thank the valuable input of Susana Pinto, Dr. Nuno Almeida, Dr. Nathalie Barroca, Dr. Clara Correia e Prof. Dr. João Mano.

Declaration of Conflicting Interests

The author(s) declared no potential conflicts of interest with respect to the research, authorship, and/or publication of this article.

Funding

This work was supported by the Portuguese funding of Program COMPETE-FEDER, Programa Operacional Competitividade e Internacionalização through the projects POCI-01-0145-FEDER-028424 and CENTRO-01-0145-FEDER-022083. Also by Fundação para a Ciência e Tecnologia I.P. (FCT, IP) through the projects PTDC/EME-SIS/28424/2017 and UID/EMS/00481/2019, and the PhD grants SFRH/BD/133129/2017 and SFRH/BD/130287/2017.

References

1. Johnstone B, Alini M, Cucchiarini M, et al. Tissue engineering for articular cartilage repair – the state of the art. *Eur Cells Mater* 2013; 25: 248–267.

2. Camarero-Espinosa S, Rothen-Rutishauser B, Foster EJ, et al. Articular cartilage: From formation to tissue engineering. *Biomater Sci* 2016; 4: 734–767.

3. Armiento AR, Stoddart MJ, Alini M, et al. Biomaterials for articular cartilage tissue engineering: Learning from biology. *Acta Biomater* 2018; 65: 1–20.

4. O'Brien FJ. Biomaterials & scaffolds for tissue engineering. *Mater Today* 2011; 14: 88–95.

5. Ghasemi-Mobarakeh L, Prabhakaran MP, Morshed M, et al. Electrospun poly(ε-caprolactone)/gelatin nanofibrous scaffolds for nerve tissue engineering. *Biomaterials* 2008; 29: 4532–4539.

6. Zheng R, Duan H, Xue J, et al. The influence of Gelatin/PCL ratio and 3-D construct shape of electrospun membranes on cartilage regeneration. *Biomaterials* 2014; 35: 152–164.

7. Kishan AP, Cosgriff-Hernandez EM. Recent advancements in electrospinning design for tissue engineering applications: A review. *J Biomed Mater Res - Part A* 2017; 105A: 2892–2905.

8. Horner CB, Low K, Nam J. Electrospun scaffolds for cartilage regeneration. In: Liu H (ed) *Nanocomposites for Musculoskeletal Tissue Regeneration*. Elsevier, pp. 213–240.

9. McCullen SD, Autefage H, Callanan A, et al. Anisotropic fibrous scaffolds for articular cartilage regeneration. *Tissue Eng Part A* 2012; 18: 2073–2083.

10. Steele JAM, McCullen SD, Callanan A, et al. Combinatorial scaffold morphologies for zonal articular cartilage engineering. *Acta Biomater* 2014; 10: 2065–2075.

11. Damanik FFR, Spadolini G, Rotmans J, et al. Biological activity of human mesenchymal stromal cells on polymeric electrospun scaffolds. *Biomater Sci* 2019; 7: 1088–1100.

12. Gautam S, Dinda AK, Mishra NC. Fabrication and characterization of PCL/gelatin composite nanofibrous scaffold for tissue engineering applications by electrospinning method. *Mater Sci Eng C* 2013; 33: 1228–1235.

13. Yao R, He J, Meng G, et al. Electrospun PCL/Gelatin composite fibrous scaffolds: Mechanical properties and cellular responses. *J Biomater Sci Polym Ed* 2016; 27: 824–838.

14. Bhattarai N, Li Z, Gunn J, et al. Natural-synthetic polyblend nanofibers for biomedical applications. *Adv Mater* 2009; 21: 2792–2797.

15. Powell HM, Boyce ST. Engineered human skin fabricated using electrospun collagen-PCL blends: morphogenesis and mechanical properties. *Tissue Eng Part A* 2009; 15: 2177–2187.

16. Aldana AA, Abraham GA. Current advances in electrospun gelatin-based scaffolds for tissue engineering applications. *Int J Pharm* 2017; 523: 441–453.

17. Zhang Y, Ouyang H, Chwee TL, et al. Electrospinning of gelatin fibers and gelatin/PCL composite fibrous scaffolds. *J Biomed Mater Res - Part B Appl Biomater* 2005; 72: 156–165.

18. Strobel HA, Calamari EL, Beliveau A, et al. Fabrication and characterization of electrospun polycaprolactone and gelatin composite cuffs for tissue engineered blood vessels. *J Biomed Mater Res - Part B Appl Biomater* 2018; 106: 817–826.

19. Alvarez-Perez MA, Guarino V, Cirillo V, et al. Influence of gelatin cues in PCL electrospun membranes on nerve outgrowth. *Biomacromolecules* 2010; 11: 2238–2246.

20. Fu W, Liu Z, Hu R, et al. Electrospun gelatin/PCL and collagen/PLCL scaffolds for vascular tissue engineering. *Int J Nanomedicine* 2014; 9: 2335–2344.

21. Ke R, Yi W, Tao S, et al. Electrospun PCL/gelatin composite nanofiber structures for effective guided bone regeneration membranes. *Mater Sci Eng C* 2017; 78: 324–332.

22. Xue J, Feng B, Zheng R, et al. Engineering ear-shaped cartilage using electrospun fibrous membranes of gelatin/polycaprolactone. *Biomaterials* 2013; 34: 2624–2631.

23. He X, Feng B, Huang C, et al. Electrospun gelatin/polycaprolactone nanofibrous membranes combined with a coculture of bone marrow stromal cells and chondrocytes for cartilage engineering. *Int J Nanomedicine* 2015; 10: 2089–2099.

24. Rnjak-Kovacina J, Weiss AS. Increasing the pore size of electrospun scaffolds. *Tissue Eng Part B Rev* 2011; 17: 365–372.

25. Hunziker EB, Quinn TM, Häuselmann HJ. Quantitative structural organization of normal adult human articular cartilage. *Osteoarthr Cartil* 2002; 10: 564–572.

26. Baker BM, Shah RP, Silverstein AM, et al. Sacrificial nanofibrous composites provide instruction without impediment and enable functional tissue formation. *Proc Natl Acad Sci* 2012; 109: 14176–14181.

27. Pham QP, Sharma U, Mikos AG. Electrospun poly (epsilon-caprolactone) microfiber and multilayer nanofiber/microfiber scaffolds: Characterization of scaffolds and measurement of cellular infiltration. *Biomacromolecules* 2006; 7: 2796–2805.

28. Formica FA, Öztürk E, Hess SC, et al. A Bioinspired Ultraporous Nanofiber-Hydrogel Mimic of the Cartilage Extracellular Matrix. *Adv Healthc Mater* 2016; 5: 3129–3138.

29. Wright LD, Andric T, Freeman JW. Utilizing NaCl to increase the porosity of electrospun materials. *Mater Sci Eng C* 2011; 31: 30–36.

30. Baker BM, Gee AO, Metter RB, et al. The potential to improve cell infiltration in composite fiber-aligned electrospun scaffolds by the selective removal of sacrificial fibers. *Biomaterials* 2008; 29: 2348–2358.

31. Wang K, Zhu M, Li T, et al. Improvement of cell infiltration in electrospun polycaprolactone scaffolds for the construction of vascular grafts. *J Biomed Nanotechnol* 2014; 10: 1–11.

32. Chong EJ, Phan TT, Lim IJ, et al. Evaluation of electrospun PCL/gelatin nanofibrous scaffold for wound healing and layered dermal reconstitution. *Acta Biomater* 2007; 3: 321–330.

33. Rose JB, Sidney LE, Patient J, et al. In vitro evaluation of electrospun blends of gelatin and PCL for application as a partial thickness corneal graft. *J Biomed Mater Res - Part A* 2019; 107: 828–838.

34. Li J, Mak AFT. Hydraulic permeability of polyglycolic acid scaffolds as a function of biomaterial degradation. *J Biomater Appl* 2005; 19: 253–266.

35. Oliver WC, Pharr GM. An improved technique for determining hardness and elastic modulus using load and displacement sensing indentation experiments. *J Mater Res* 1992; 7: 1564–1583.

36. Gil-Castell O, Badia JD, Ribes-Greus A. Tailored electrospun nanofibrous polycaprolactone/gelatin scaffolds into an acid hydrolytic solvent system. *Eur Polym J* 2018; 101: 273–281.

37. Skotak M, Ragusa J, Gonzalez D, et al. Improved cellular infiltration into nanofibrous electrospun cross- linked gelatin scaffolds templated with micrometer sized polyethylene glycol fibers. *Biomed Mater* 2011; 6: 055012.

38. Butcher AL, Koh CT, Oyen ML. Systematic mechanical evaluation of electrospun gelatin meshes. *J Mech Behav Biomed Mater* 2017; 69: 412–419.

39. Stockwell RA. Chondrocytes. *J Clin Pathol* 1978; s3-12: 7–13.

40. Erencia M, Cano F, Tornero JA, et al. Preparation of electrospun nanofibers from solutions of different gelatin types using a benign solvent mixture composed of water/PBS/ethanol. *Polym Adv Technol* 2016; 27: 382–392.

41. Ratajska-Gadomska B, Gadomski W. Influence of confinement on solvation of ethanol in water studied by Raman spectroscopy. *J Chem Phys* 2010; 133: 234505.

42. Munj HR, Lannutti JJ, Tomasko DL. Understanding drug release from PCL/gelatin electrospun blends. *J Biomater Appl* 2017; 31: 933–949.

43. Little CJ, Bawolin NK, Chen X. Mechanical properties of natural cartilage and tissue-engineered constructs. *Tissue Eng Part B Rev* 2011; 17: 213–227.

44. Tripathi A, Melo JS. Preparation of a sponge-like biocomposite agarose-chitosan scaffold with primary hepatocytes for establishing an in vitro 3D liver tissue model. *RSC Adv* 2015; 5: 30701–30710.

45. Jeong CG, Zhang H, Hollister SJ. Three-dimensional poly(1,8-octanediol-co-citrate) scaffold pore shape and permeability effects on sub-cutaneous in vivo chondrogenesis using primary chondrocytes. *Acta Biomater* 2011; 7: 505–514.

46. Cho D, Chen S, Jeong Y, et al. Surface hydro-properties of electrospun fiber mats. *Fibers Polym* 2015; 16: 1578–1586.

47. Elzein T, Nasser-Eddine M, Delaite C, et al. FTIR study of polycaprolactone chain organization at interfaces. *J Colloid Interface Sci* 2004; 273: 381–387.

48. Lim YC, Johnson J, Fei Z, et al. Micropatterning and characterization of electrospun poly(ε-caprolactone)/gelatin nanofiber tissue scaffolds by femtosecond laser ablation for tissue engineering applications. *Biotechnol Bioeng* 2011; 108: 116–126.

49. Mohammadzadehmoghadam S, Dong Y. Fabrication and Characterization of Electrospun Silk Fibroin/Gelatin Scaffolds Crosslinked With Glutaraldehyde Vapor. *Front Mater* 2019; 6: 1–12.

50. Dulnik J, Denis P, Sajkiewicz P, et al. Biodegradation of bicomponent PCL/gelatin and PCL/collagen nanofibers electrospun from alternative solvent system. *Polym Degrad Stab* 2016; 130: 10–21.

51. Chieng B, Ibrahim N, Yunus W, et al. Poly(lactic acid)/Poly(ethylene glycol) Polymer Nanocomposites: Effects of Graphene Nanoplatelets. *Polymers (Basel)* 2013; 6: 93–104.

52. Chen C, Liu K, Wang H, et al. Morphology and performances of electrospun polyethylene glycol/poly (dl-lactide) phase change ultrafine fibers for thermal energy storage. *Sol Energy Mater Sol Cells* 2013; 117: 372–381.

53. Pramanik S, Ataollahi F, Pingguan-Murphy B, et al. In vitro study of surface modified poly(ethylene glycol)-impregnated sintered bovine bone scaffolds on human fibroblast cells. *Sci Rep* 2015; 5: 1–11.

54. Zhou Q, Zhang H, Zhou Y, et al. Alkali-Mediated Miscibility of Gelatin/Polycaprolactone for Electrospinning Homogeneous Composite Nanofibers for Tissue Scaffolding. *Macromol Biosci* 2017; 17: 1–10.

55. Wong SC, Baji A, Leng S. Effect of fiber diameter on tensile properties of electrospun poly(ε-caprolactone). *Polymer (Guildf)* 2008; 49: 4713–4722.

56. Gong M, Chi C, Ye J, et al. Icariin-loaded electrospun PCL/gelatin nanofiber membrane as potential artificial periosteum. *Colloids Surfaces B Biointerfaces* 2018; 170: 201–209.

57. Wang J, Yuan B, Han RPS. Modulus of elasticity of randomly and aligned polymeric scaffolds with fiber size dependency. *J Mech Behav Biomed Mater* 2018; 77: 314–320.

58. Bellucci G, Seedhom BB. Mechanical behaviour of articular cartilage under tensile cyclic load. *Rheumatology* 2001; 40: 1337–1345.

59. Boi M, Marchiori G, Berni M, et al. Nanoindentation: An advanced procedure to investigate osteochondral engineered tissues. *J Mech Behav Biomed Mater* 2019; 96: 79–87.

60. Jung JW, Lee H, Hong JM, et al. A new method of fabricating a blend scaffold using an indirect three-dimensional printing technique. *Biofabrication* 2015; 7: 045003.

61. Stolz M, Gottardi R, Raiteri R, et al. Early detection of aging cartilage and osteoarthritis in mice and patient samples using atomic force microscopy. *Nat Nanotechnol* 2009; 4: 186–192.

62. Antons J, Marascio MGM, Nohava J, et al. Zone-dependent mechanical properties of human articular cartilage obtained by indentation measurements. *J Mater Sci Mater Med*; 29:57.

63. Divieto C, Sassi MP. A first approach to evaluate the cell dose in highly porous scaffolds by using a nondestructive metabolic method. *Futur Sci OA* 2015; 1: FSO58.

64. Feng B, Tu H, Yuan H, et al. Acetic-acid-mediated miscibility toward electrospinning homogeneous composite nanofibers of GT/PCL. *Biomacromolecules* 2012; 13: 3917–3925.

65. Wang K, Xu M, Zhu M, et al. Creation of macropores in electrospun silk fibroin scaffolds using sacrificial PEO-microparticles to enhance cellular infiltration. *J Biomed Mater Res - Part A* 2013; 101: 3474–3481.

66. Fee T, Surianarayanan S, Downs C, et al. Nanofiber Alignment Regulates NIH3T3 Cell Orientation and Cytoskeletal Gene Expression on Electrospun PCL+Gelatin Nanofibers. *PLoS One* 2016; 11: e0154806.